

First-principles residual resistivity using a locally self-consistent multiple scattering methodVishnu Raghuraman  and Michael Widom *Department of Physics, Carnegie Mellon University, Pittsburgh, Pennsylvania 15213, USA*Markus Eisenbach *National Center for Computational Sciences, Oak Ridge National Laboratory, Oak Ridge, Tennessee 37831, USA*Yang Wang *Pittsburgh Supercomputing Center, Carnegie Mellon University, Pittsburgh, Pennsylvania 15213, USA*

(Received 7 December 2023; accepted 23 February 2024; published 15 March 2024)

The locally self-consistent multiple scattering (LSMS) method can perform efficient first-principles calculations of systems with a large number of atoms. In this paper, we combine the Kubo-Greenwood equation with LSMS, enabling us to calculate the first-principles residual resistivity of large systems. This has been implemented in the open-source code LSMS. We apply this method to selected pure elements and binary random alloys. The results compare well with experiment, and with values obtained from a first-principles effective medium technique (the Korringa-Kohn-Rostoker coherent potential approximation). We discuss future applications of this method to complex systems where other methods are not applicable.

DOI: [10.1103/PhysRevB.109.104204](https://doi.org/10.1103/PhysRevB.109.104204)**I. INTRODUCTION**

Disordered systems show interesting physical and chemical properties [1–3]. Multiprincipal element alloys with high chemical disorder have shown high strength and ductility over large temperature ranges [4–6]. Bulk metallic glasses exhibit ultrahigh strength, high elasticity, high fracture toughness, high wear resistance, and other useful properties [7,8]. Quasicrystals possess high thermal and electrical resistivity, low adhesion, and have been used as the coating for nonstick cookware [9]. First-principles density functional theory allows us to compute phase behavior, band structure, mechanical, and functional properties for these systems [10–12]. However, the computational cost of standard density functional theory (DFT) calculations grows as the cube of the system size, making the study of large systems impractical. It is possible to use an effective medium method, such as the coherent potential approximation (CPA) [13] to model the system using few atoms. While this works well for chemical species disorder, it is difficult to construct an effective medium for atomic displacements, or other forms of disorder which break crystallinity. Alternatively, we can perform classical molecular dynamics (MD) using potentials fitted against DFT data. This approach is significantly faster in comparison to DFT, however, obtaining these potentials is a highly difficult task, especially for complex systems, and classical MD yields no information concerning the electronic structure.

The locally self-consistent multiple scattering (LSMS) method [14], based on the Korringa-Kohn-Rostoker (KKR) Green's function approach to DFT [15,16], offers an efficient solution to this problem. As in the KKR method, LSMS uses multiple scattering theory to obtain the Green's function of the system. However, electron scattering between widely

separated atoms is ignored. The cutoff distance for nonzero scattering is represented by the local interaction zone (LIZ) radius. This approximation speeds up the calculation significantly. LSMS scales linearly with the system size, making it a practical computational tool for disorder studies. Furthermore, the LSMS approach provides a natural domain decomposition of the system and thus enables the highly efficient use of massively parallel computing architectures and accelerators [17].

The KKR Green's function method can be combined with the Kubo-Greenwood linear response formula [18,19] to obtain first-principles electrical conductivity. The Kubo-Greenwood equation depends on products of Green's functions, which are readily available in KKR. For a random system, this product must be averaged over the ensemble. Butler [20] showed that the ensemble average can be treated using the CPA medium. The KKR-CPA conductivity method has since been applied successfully to several systems [21–23]. Alternatively, we can represent the ensemble average using a single, carefully constructed large structure. The Green's function for this system can be calculated using LSMS and inserted into the Kubo-Greenwood equation, which produces the electrical conductivity. This linear scaling nature of LSMS enables us to apply this approach to systems with tens of thousands of atoms, allowing us to calculate conductivity for structures with intricate features such as stacking faults, dislocations, and quasicrystalline order. We have implemented this in the open source high-performance software package LSMS [24]. The resulting conductivity depends on the LIZ radius, and convergence with the LIZ radius will be a major point of discussion in this paper.

The next section provides some theoretical background on the LSMS method and the Kubo-Greenwood equation. We

then introduce our LSMS resistivity approach and provide a heuristic derivation for the conductivity as a function of the LIZ radius. We test our method by applying it to selected pure elements with a variety of structural and electronic characteristics (Ag, Al, Li, and V) and binary alloys ($\text{Al}_x\text{V}_{1-x}$ and Fe-9 wt % Si). We compare the results with experimental data and computational values obtained from KKR-CPA. Finally, we conclude by discussing areas of improvements for the method and potential future applications.

II. METHODS

A. KKR and LSMS

The Korringa-Kohn-Rostoker (KKR) approach to density functional theory solves for the Green's function of the Kohn-Sham equation [25,26]. The charge density can be obtained from the Green's function using

$$\rho(\mathbf{r}) = -\frac{1}{\pi} \int_{-\infty}^{\epsilon_F} d\epsilon \text{Im}\{\text{Tr}[G(\mathbf{r}, \mathbf{r}, \epsilon)]\}, \quad (1)$$

which is then used to calculate a new Hamiltonian. Using multiple scattering theory, we express the Green's function in the vicinity of atomic site n as [27,28]

$$G(\mathbf{r}_n, \mathbf{r}_n, \epsilon) = \sum_{L'L} Z_L^n(\mathbf{r}_n, \epsilon) \tau_{L'L}^{mn}(\epsilon) Z_{L'}^n(\mathbf{r}_n) - \sum_L Z_L^n(\mathbf{r}_n, \epsilon) J_L^{n*}(\mathbf{r}_n, \epsilon), \quad (2)$$

where Z^n and J^n are the regular and irregular solutions to the single-atom Schrödinger equation for the atom at site n . L and L' are angular momentum indices [e.g., $L \equiv (lm)$]. Note that for real energies, the second term in Eq. (2) is real and does not affect the imaginary part of the Green's function. The multiple scattering path matrix τ can be expressed in terms of the single-site scattering t matrix and the free-electron propagator g as [29]

$$\underline{\tau}^{mn} = ([\underline{T}^{-1} - \underline{g}]^{-1})^{mn}, \quad (3)$$

$$\underline{T}^{mn} = \underline{t}^m \delta^{mn}. \quad (4)$$

Here, m and n refer to atomic sites. Formally, τ obeys a Dyson expansion

$$\tau^{mn} = t^m \delta^{mn} + t^m g^{mn} t^n + \sum_{k \neq m, n} t^m g^{mk} t^k g^{kn} t^n + \dots \quad (5)$$

$$= t^m \delta^{mn} + t^m g^{mk} \tau^{kn}. \quad (6)$$

Calculating the matrix inverse in Eq. (3) is the most computationally intensive step in the KKR method. This operation scales as the cube of the number of atoms in the system. In LSMS, we define a local interaction zone (LIZ) for each atom, beyond which scattering is neglected (Fig. 1). This results in a much smaller τ matrix, and the inverse scales linearly with the system size. It is important to choose an appropriate value of LIZ radius. A large LIZ radius slows down the calculation, while a small LIZ radius produces inaccurate results. For a given system, it is important to test multiple LIZ radii to ensure convergence.

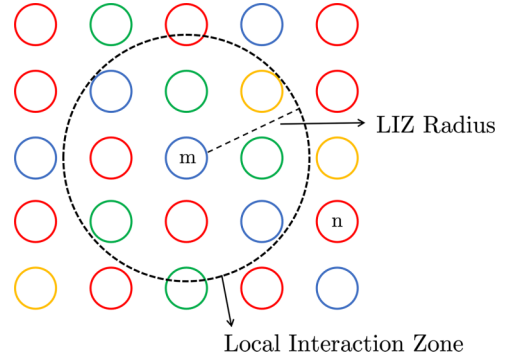


FIG. 1. Schematic depiction the local interaction zone (LIZ) for an atom m . Scattering between m and any atom n beyond the LIZ is ignored ($\tau^{mn} = 0$).

B. Conductivity

Electrical conductivity obeys the Kubo-Greenwood equation [20]

$$\sigma_{\mu\nu} = \frac{1}{4} \lim_{\delta \rightarrow 0} [\tilde{\sigma}_{\mu\nu}(\epsilon_F + i\delta, \epsilon_F + i\delta) - \tilde{\sigma}_{\mu\nu}(\epsilon_F + i\delta, \epsilon_F - i\delta) - \tilde{\sigma}_{\mu\nu}(\epsilon_F - i\delta, \epsilon_F + i\delta) + \tilde{\sigma}_{\mu\nu}(\epsilon_F - i\delta, \epsilon_F - i\delta)], \quad (7)$$

$$\tilde{\sigma}_{\mu\nu}(z_1, z_2) = -\frac{\hbar}{\pi N \Omega} \text{Tr}(j_\mu G(z_1) j_\nu G(z_2)), \quad (8)$$

where μ and ν refer to Cartesian directions, j_μ and j_ν are current operators, N is the number of atoms, and Ω is the atomic volume. The angular brackets represent an ensemble average over different random configurations. We express this equation in terms of multiple scattering matrices as [20]

$$\tilde{\sigma}_{\mu\nu}(z_1, z_2) = -\frac{4m_e^2}{\pi N \Omega \hbar^3} \sum_{mm} \sum_{L_1 L_2 L_3 L_4} \langle J_{L_4 L_1}^{m\mu}(z_2, z_1) \tau_{L_1 L_2}^{mn} \times (z_1) J_{L_2 L_3}^{n\nu}(z_1, z_2) \tau_{L_3 L_4}^{nm}(z_2) \rangle, \quad (9)$$

where J is the matrix element of the current operator. Since the sum over m generates a volume average, we replace the ensemble average with a single, sufficiently large and representative, random structure. Additionally, for each atom m , we only consider atoms n within the LIZ of m . Within the LSMS formalism,

$$\tilde{\sigma}_{\mu\nu}(z_1, z_2) = -\frac{4m_e^2}{\pi N \Omega \hbar^3} \sum_m \sum_n^{\text{LIZ}_m} \sum_{L_1 L_2 L_3 L_4} J_{L_4 L_1}^{m\mu}(z_2, z_1) \tau_{L_1 L_2}^{mn}(z_1) \times J_{L_2 L_3}^{n\nu}(z_1, z_2) \tau_{L_3 L_4}^{nm}(z_2). \quad (10)$$

Combining Eqs. (10) and (7) yields the LSMS electrical conductivity tensor for a given LIZ size, which is then inverted to obtain the resistivity.

C. Dependence on LIZ radius

Because our LIZ sizes are limited by available computing resources, we wish to model the convergence of conductivity with increasing LIZ size. Here, we derive this dependence heuristically. Consider a perfectly periodic crystal for which the electron mean free path is infinite. Assuming weak scattering, and truncating the Dyson expansion Eq. (6) at first

order in g , we find the $L = 0$ component of the τ matrix varies asymptotically as

$$\tau_{L_1 L_2}(r, z) \approx \beta_{L_1 L_2}(z) \frac{e^{ikr}}{r}, \quad (11)$$

where $\kappa = \sqrt{2m_e z / \hbar^2}$.

Replacing the sums in Eq. (10) with integrals, the conductivity components $\tilde{\sigma}(z_1, z_2)$ can be expressed as

$$\tilde{\sigma}_{\mu\nu}(z_1, z_2) \approx A(z_1, z_2) \int_{r_c}^{r_{\text{LIZ}}} dr r^2 \left(\frac{e^{ik_1 r}}{r} \right) \left(\frac{e^{ik_2 r}}{r} \right), \quad (12)$$

where $\kappa_{1,2} = \sqrt{2m_e z_{1,2} / \hbar^2}$, r_c is the nearest-neighbor separation, and r_{LIZ} is the LIZ radius. We can integrate this to obtain the four terms needed for conductivity,

$$\tilde{\sigma}_{\mu\nu}(r_{\text{LIZ}}, \epsilon_+, \epsilon_+) \approx \frac{A_{++}}{\kappa_+} e^{i\kappa_+(r_{\text{LIZ}}+r_c)} \sin[\kappa_+(r_{\text{LIZ}} - r_c)], \quad (13)$$

$$\tilde{\sigma}_{\mu\nu}(r_{\text{LIZ}}, \epsilon_+, \epsilon_-) \approx A_{+-}[r_{\text{LIZ}} - r_c], \quad (14)$$

$$\tilde{\sigma}_{\mu\nu}(r_{\text{LIZ}}, \epsilon_-, \epsilon_+) \approx A_{-+}[r_{\text{LIZ}} - r_c], \quad (15)$$

$$\tilde{\sigma}_{\mu\nu}(r_{\text{LIZ}}, \epsilon_-, \epsilon_-) \approx \frac{A_{--}}{\kappa_+} e^{-i\kappa_+(r_{\text{LIZ}}+r_c)} \sin[\kappa_+(r_{\text{LIZ}} - r_c)], \quad (16)$$

where $\epsilon_{+-} = \epsilon_F \pm i\delta$, $\kappa_+ = \sqrt{2m_e \epsilon_+ / \hbar^2}$, and we have taken the limit $\delta \rightarrow 0$. The conductivity is given by

$$\sigma_{\mu\nu} \approx -\frac{[A_{+-} + A_{-+}]}{4} (r_{\text{LIZ}} - r_c) + \frac{\sin[\kappa_+(r_{\text{LIZ}} - r_c)]}{4\kappa_+} \times [A_{++} e^{i\kappa_+(r_{\text{LIZ}}-r_c)} + A_{--} e^{i\kappa_-(r_{\text{LIZ}}-r_c)}]. \quad (17)$$

The conductivity shows a combination of linear and oscillatory behavior. The oscillations occur at frequency $2k_F$ with k_F the Fermi wave number. At large r_{LIZ} the linear term dominates, the conductivity diverges, and the resistivity vanishes, as expected for perfectly crystalline systems. In particular, the resistivity vanishes linearly as a function of the inverse LIZ radius.

In order for the conductivity to converge, the τ matrix must decay faster than $1/r$. To model systems with finite conductivity, consider the following ansatz,

$$\tau_{L_1 L_2}(z) \approx \beta_{L_1 L_2}(z) \frac{e^{ikr}}{r} e^{-\alpha r}, \quad (18)$$

where α is a decay parameter determined by the inverse of the mean free path. For weak disorder, $\alpha \rightarrow 0$, and we recover the linear conductivity expression. For disordered systems, $\alpha > 0$, and the conductivity component $\tilde{\sigma}$ becomes

$$\tilde{\sigma}_{\mu\nu}(z_1, z_2) \approx A(z_1, z_2) \int_{r_c}^{r_{\text{LIZ}}} dr r^2 \left(\frac{e^{ik_1 r}}{r} \right) \left(\frac{e^{ik_2 r}}{r} \right) e^{-2\alpha r}, \quad (19)$$

resulting in

$$\tilde{\sigma}_{\mu\nu}(\epsilon_+, \epsilon_+) \approx A_{++} \left[\frac{e^{(2i\kappa_+ - 2\alpha)r_{\text{LIZ}}} - e^{(2i\kappa_+ - 2\alpha)r_c}}{2i\kappa_+ - 2\alpha} \right], \quad (20)$$

$$\tilde{\sigma}_{\mu\nu}(\epsilon_+, \epsilon_-) \approx A_{+-} \left[\frac{e^{-2\alpha r_c} - e^{-2\alpha r_{\text{LIZ}}}}{2\alpha} \right], \quad (21)$$

$$\tilde{\sigma}_{\mu\nu}(\epsilon_-, \epsilon_+) \approx A_{-+} \left[\frac{e^{-2\alpha r_c} - e^{-2\alpha r_{\text{LIZ}}}}{2\alpha} \right], \quad (22)$$

$$\tilde{\sigma}_{\mu\nu}(\epsilon_-, \epsilon_-) \approx A_{--} \left[\frac{e^{-(2i\kappa_+ + 2\alpha)r_{\text{LIZ}}} - e^{-(2i\kappa_+ + 2\alpha)r_c}}{-2i\kappa_+ - 2\alpha} \right]. \quad (23)$$

Note the combination of oscillating and exponentially decayed terms. The conductivity approaches a finite limit as

$$\sigma_{\mu\nu} \approx a_0 e^{-2\alpha r_{\text{LIZ}}} + a_1, \quad (24)$$

where

$$a_0 = \frac{1}{4} \left[\frac{A_{++}}{2i\kappa_+ - 2\alpha} e^{2i\kappa_+ r_{\text{LIZ}}} - \frac{A_{--}}{2i\kappa_+ + 2\alpha} e^{-2i\kappa_+ r_{\text{LIZ}}} + \frac{(A_{+-} + A_{-+})}{2\alpha} \right], \quad (25)$$

$$a_1 = -\frac{1}{4} \left[\frac{A_{++}}{2i\kappa_+ - 2\alpha} e^{2i\kappa_+ r_c} - \frac{A_{--}}{2i\kappa_+ + 2\alpha} e^{-2i\kappa_+ r_c} + \frac{(A_{+-} + A_{-+})}{2\alpha} \right] e^{-2\alpha r_c}. \quad (26)$$

The resistivity is now finite, and its dependence on the inverse LIZ size is *nonlinear*. It is possible to show that when $\alpha \rightarrow 0$ and $r_{\text{LIZ}} \rightarrow \infty$ (with αr_{LIZ} finite), the conductivity becomes infinite. When $\alpha \rightarrow 0$, we can write

$$a_0 \approx \frac{A_{+-} + A_{-+}}{8\alpha}, \quad a_1 \approx -\frac{A_{+-} + A_{-+}}{8\alpha} e^{-2\alpha r_c}, \quad (27)$$

$$a_0 \approx -a_1 e^{2\alpha r_c}.$$

Inserting these expressions in (24), we get

$$\sigma_{\mu\nu} \approx a_1 (1 - e^{-2\alpha(r_{\text{LIZ}}-r_c)}) \approx -e^{-2\alpha r_c} (A_{+-} + A_{-+}) \frac{1 - e^{-2\alpha(r_{\text{LIZ}}-r_c)}}{8\alpha}. \quad (28)$$

Now, since the product αr_{LIZ} will be finite, the numerator $(1 - e^{-2\alpha(r_{\text{LIZ}}-r_c)})$ will be finite, while the denominator is 0. This means that the conductivity will be infinite when $\alpha \rightarrow 0$ and $r_{\text{LIZ}} \rightarrow \infty$, which is expected.

However, if $\alpha \rightarrow 0$ and r_{LIZ} is finite, such that αr_{LIZ} is small, we can expand the exponential up to first order in αr_{LIZ} , resulting in

$$\sigma_{\mu\nu} \approx -\frac{1}{4} e^{-2\alpha r_c} (A_{+-} + A_{-+}) (r_{\text{LIZ}} - r_c). \quad (29)$$

This shows that the conductivity varies linearly with r_{LIZ} in the regime where αr_{LIZ} is small.

Finally, we can write a linear expression for resistivity where $\alpha \rightarrow 0$ and $r_{\text{LIZ}} \ll \alpha^{-1}$. In this regime, the conductivity can be expressed as

$$\sigma_{\mu\nu} \approx a_1 (1 - e^{-2\alpha(r_{\text{LIZ}}-r_c)}) \quad (30)$$

$$\approx a_1 \frac{e^{2\alpha(r_{\text{LIZ}}-r_c)} - 1}{e^{2\alpha(r_{\text{LIZ}}-r_c)}} \quad (31)$$

$$\approx \frac{2a_1 \alpha (r_{\text{LIZ}} - r_c)}{1 + 2\alpha (r_{\text{LIZ}} - r_c)}. \quad (32)$$

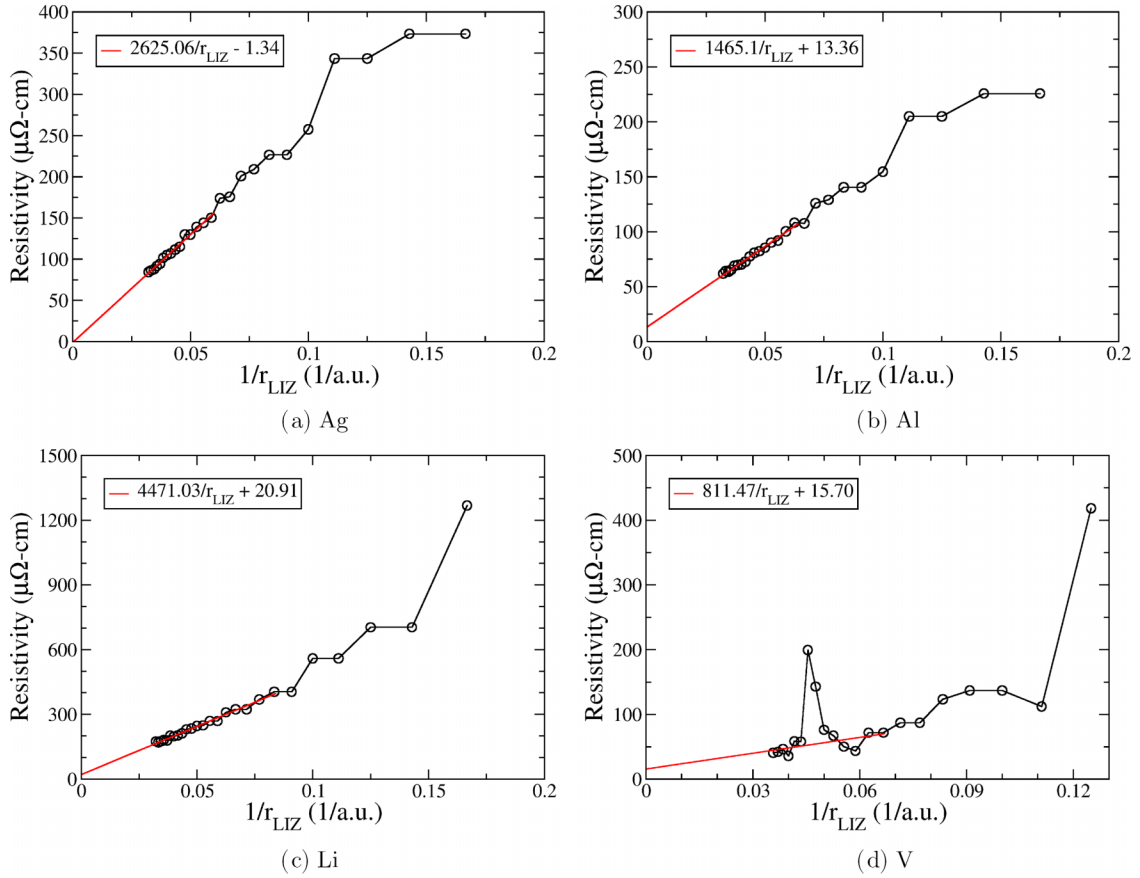


FIG. 2. The resistivity of pure elements as a function of the local interaction zone radius. A linear extrapolation is applied based on a small scattering approximation.

To recover the linearity of resistivity for weak scattering, invert σ to obtain

$$\rho_{\mu\nu} \approx \frac{1 + 2\alpha(r_{\text{LIZ}} - r_c)}{2\alpha a_1(r_{\text{LIZ}} - r_c)} \quad (33)$$

$$\approx \frac{1}{2\alpha a_1} k_{\text{LIZ}} + \frac{1}{a_1}, \quad k_{\text{LIZ}} = \frac{1}{r_{\text{LIZ}} - r_c}. \quad (34)$$

In the small α regime, the resistivity varies linearly with the inverse of the LIZ radius. However, the linear expression is only valid for $r_{\text{LIZ}} \ll \alpha^{-1}$. But as $\alpha \rightarrow 0$, the LIZ radius range over which we see linearity will increase. As a result, using the linear expression in lieu of the full nonlinear form might result in smaller errors. We will explore this idea further in the next section when we discuss the resistivity of binary random alloys.

III. COMPUTATIONAL DETAILS

We apply the LSMS resistivity method (as implemented in the open source code LSMS) to a $20 \times 20 \times 20$ supercell (16 000 atoms) for bcc structures and a $16 \times 16 \times 16$ supercell (16 384 atoms) for fcc structures. A suitable starting potential is needed for resistivity calculations. For the pure elements and $\text{Al}_x\text{V}_{1-x}$ binaries, we perform self-consistent LSMS calculations to obtain a converged potential. For FeSi, we obtain converged atomic potentials for Fe and Si from a KKR-CPA calculation. We employ the von Barth–Hedin local

density approximation [25,30] for the exchange-correlation functional. The angular momentum cutoff l_{max} was set to 3. KKR-CPA calculations were performed using the open source code MUST [31]. For FeSi, we perform spin-polarized calculations. Computationally intensive sections of the calculations are GPU accelerated. All LSMS calculations are performed on the Frontier supercomputer at Oak Ridge National Laboratory. The calculations are highly efficient and scalable—using 1 GPU per atom, we are able to calculate resistivity for a 16 000-atom structure with approximately a 1000-atom LIZ in under 10 min.

IV. RESULTS

A. Pure elements

For a pure element at 0 K, the residual resistivity should vanish. We calculate LSMS resistivity of some pure elements as a basic test of the method. Figure 2 shows the resistivity of pure Ag, Li, Al, and V as a function of the inverse local interaction zone radius, represented in atomic units (1 a.u. = 0.5291 Å). In Ag and Li, the transport behavior is dominated by the valence s electrons, while V has d -electron valence and Al has both s - and p -electron valence. Due to finite memory, extrapolation is necessary to obtain the resistivity at the asymptotic limit ($1/r_{\text{LIZ}} \rightarrow 0$). Based on the heuristic expressions derived in the previous section, we apply a linear extrapolation to obtain the resistivity at infinite LIZ

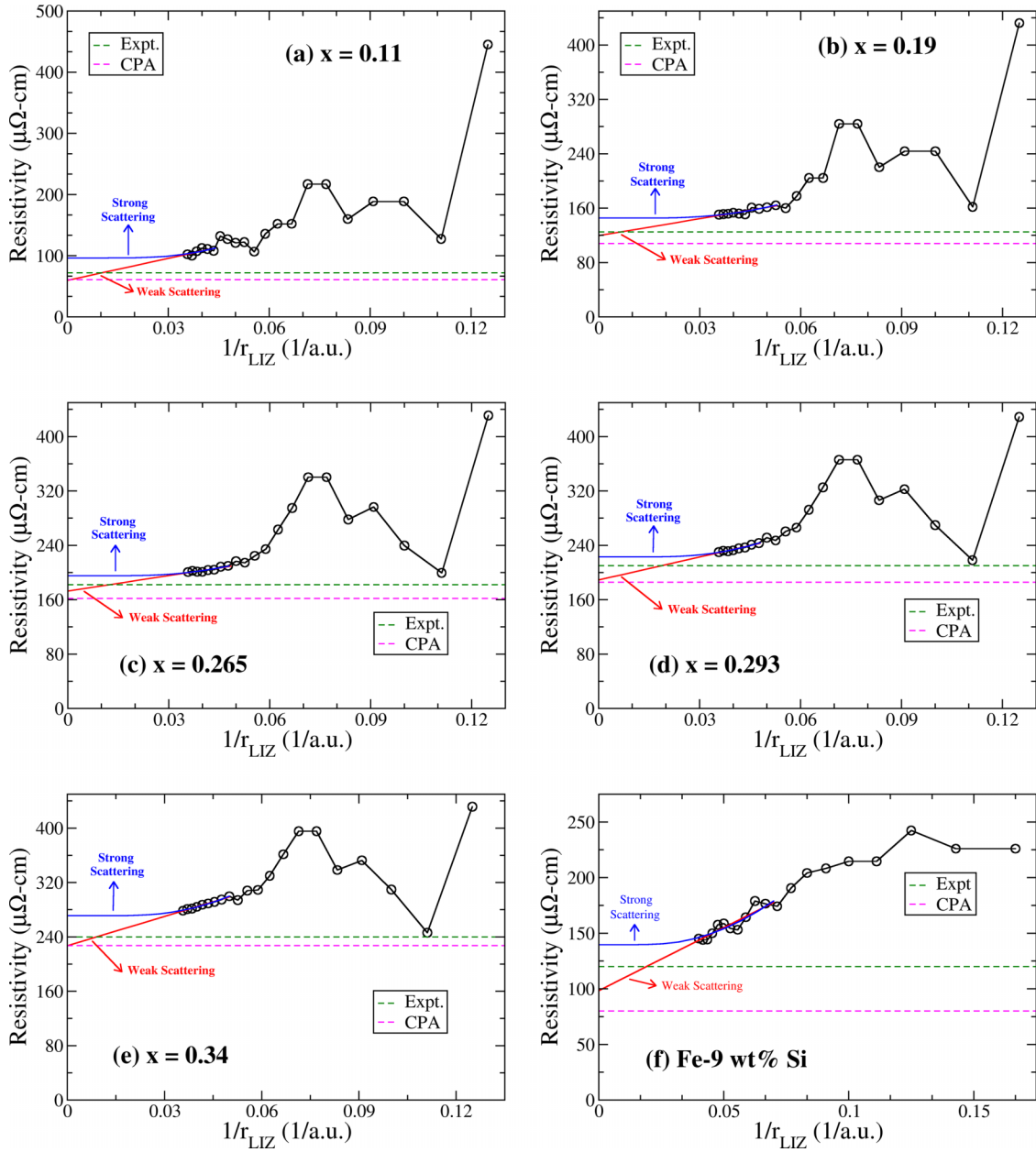


FIG. 3. Resistivity of (a)–(e) $\text{Al}_x\text{V}_{1-x}$ and (f) Fe-9 wt % Si as a function of the local interaction zone radius, denoted by the black line with circles. The experimental value is denoted by the dotted green line [33,34]. Upper bound (blue line) and lower bound (red line) heuristic functional forms are fit and extrapolated to obtain the residual resistivity.

radius. For most of the pure elements, the trends observed in Fig. 2 obey our expectations. Vanadium shows anomalous behavior—there is a sharp peak which is not explained by the small scattering approximation. The extrapolated residual resistivity is small for all the cases. Since our heuristic models only produce the functional form, we are unable to determine why there is a slight underestimate for Ag but an overestimate for the other cases. More complex theoretical models are required to further understand these trends.

B. Binary alloys

For random alloys, we expect the resistivity to decay exponentially to a nonzero value, in accordance with the heuristic

derived in the previous section. Inverting the conductivity in Eq. (30) yields

$$\rho_{\mu\nu} = \frac{b_0}{1 + b_1 e^{-2\alpha r_{\text{LIZ}}}}. \quad (35)$$

Figures 3(a)–3(e) show the resistivity as a function of the inverse LIZ radius for bcc $\text{Al}_x\text{V}_{1-x}$ where $x = 0.11, 0.19, 0.265, 0.293,$ and 0.34 . The strong linear trend in the data implies that the nonlinear regime has not been reached. Hence, the α parameter cannot be determined by fitting the heuristic—any α value would yield an acceptable fit to the linear trend. Instead, we define a range for α , which we use to establish upper and lower bounds. We know that α is inversely proportional to the mean free path. In the strong scattering limit, the mean free

TABLE I. b_0, b_1, c_0, c_1 coefficients [defined in Eqs. (36) and (37)] for $\text{Al}_x\text{V}_{1-x}$ and Fe-9 wt % Si.

System	Strong scattering function $\rho(r_{\text{LIZ}}) = b_0/(1 + b_1 e^{-0.15r_{\text{LIZ}}})$		Weak scattering function $\rho(r_{\text{LIZ}}) = c_0 + c_1/r_{\text{LIZ}}$	
	b_0 ($\mu\Omega$ cm)	b_1	c_0 ($\mu\Omega$ cm)	c_1 ($\mu\Omega$ cm bohr)
$\text{Al}_{0.11}\text{V}_{0.89}$	108	3.41	67	1265
$\text{Al}_{0.19}\text{V}_{0.81}$	157	2.45	119	1207
$\text{Al}_{0.265}\text{V}_{0.735}$	225	2.74	174	1667
$\text{Al}_{0.293}\text{V}_{0.707}$	268	1.83	215	1663
$\text{Al}_{0.34}\text{V}_{0.66}$	322	1.63	278	1442
Fe-9 wt % Si	140	1.87	98	1133

path is expected to be close to the lattice spacing [32]. The strong scattering function should also fit the linear trend, and become nonlinear almost immediately after the last data point. We choose $2\alpha_{\text{max}} = 0.15 \text{ \AA}^{-1}$ (corresponding to a mean free path of 6–7 \AA), producing the exponentially varying upper bound function

$$\rho_{\mu\nu}^{\text{upper}} = \frac{b_0}{1 + b_1 e^{-0.15r_{\text{LIZ}}}}. \quad (36)$$

In the weak scattering limit, the resistivity will show nonlinearity at a very large r_{LIZ} . As a result, it will appear nearly linear and we can apply the linear fitting equation

$$\rho_{\mu\nu}^{\text{lower}} \approx c_0 + c_1 \frac{1}{r_{\text{LIZ}}}, \quad (37)$$

which is similar to Eq. (34), with $r_c \rightarrow 0$. Note that in this scenario the system has a finite (but small) α and we expect finite resistivity, given by c_0 . Table I contains values for the $b_0, b_1, c_0,$ and c_1 coefficients for $\text{Al}_x\text{V}_{1-x}$ obtained by fitting the LSMS resistivity. The resistivity as a function of the LIZ radius can be bounded between the upper and lower bound functions

$$\rho_{\mu\nu}^{\text{lower}} \leq \rho_{\mu\nu} \leq \rho_{\mu\nu}^{\text{upper}}. \quad (38)$$

We also calculate first principles residual resistivity within the KKR-CPA method effective medium model of the random alloy. Figure 4 compares the extrapolated upper and lower bound LSMS resistivity to the experimental and CPA values. The experimental values [33] lie between the two bounds for all the cases. The lower bound values compare very well with the experimental and CPA values. The upper bound values in some cases also compare well with the experiment. At all concentrations, the CPA values underestimate the resistivity, which is a well-known feature of resistivities obtained from KKR-CPA [22].

We also calculate the resistivity of bcc Fe-9 wt % Si alloy [Fig. 3(f)]. A collinear spin-polarized calculation was performed where the contribution of the spin-up and spin-down electrons to the conductivity was calculated separately and summed. The experimental value [34] again lies between the lower and upper bound estimates. The fact that both the LSMS lower bound and KKR-CPA underestimate the resistivity is expected since the experimental values were obtained at room temperature.

V. CONCLUSION

In this paper, we introduce the LSMS-Kubo-Greenwood technique, which combines the Kubo-Greenwood equation with first-principles LSMS theory. Restricting scattering within finite *local interaction zones* allows efficient calculation of electrical resistivity for very large systems. We implement this method in the high-performance open source code LSMS. Using a heuristic approach, we demonstrated that the conductivity should grow linearly with respect to LIZ radius and diverge for pure elements, but converge nonlinearly for random alloys. The convergence is controlled by a parameter α , that depends on the mean free path. In the weak scattering regime, a convergent linear expression was obtained. We test the method by applying it to pure elements, where a linear trend that extrapolates to low resistivity was confirmed. We also apply this method to binary random alloys $\text{Al}_x\text{V}_{1-x}$ and Fe-9 wt % Si. A linear trend was also observed in these systems which was fitted to obtain the upper and lower bounds for the resistivity. Experimental resistivities were found to lie between the two bounds, with the lower bound values comparing well with experimental and KKR-CPA values. This demonstrates the validity of our approach.

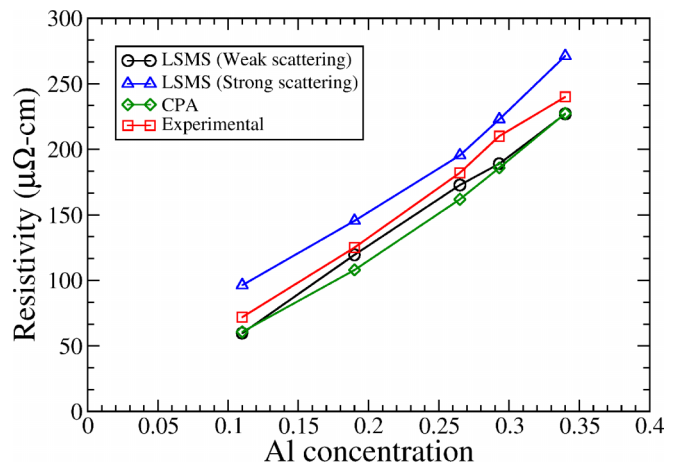


FIG. 4. Residual resistivity of bcc $\text{Al}_x\text{V}_{1-x}$ as function of x . The black circles represent lower bound values calculated using the LSMS resistivity method, while the blue triangles represent the upper bound values. The green circles represent resistivity obtained using the coherent potential approximation (CPA), and the red squares represent the experimental values [33].

Our theory and implementation of LSMS conductivity requires further improvement. While we are able to efficiently calculate resistivity for large unit cells and LIZ sizes of up to 1000 atoms, it should be possible to improve the code to allow for even larger LIZ sizes. Our heuristic approach is useful to understand the general trend and obtain upper and lower bounds. However, a more precise functional form for the resistivity should be derived without introducing any *ad hoc* parameters.

The ability to deal with a large number of atoms opens the door for several exciting applications. LSMS can be used to calculate the resistivity as a function of short-range ordering in high entropy alloys. We can study the effect of stacking faults, dislocations, and other defects on the electrical resistivity. We can also use LSMS to calculate the transport properties

of noncrystalline systems such as quasicrystals and metallic glasses. These applications are the subject of ongoing work.

ACKNOWLEDGMENTS

This work was supported by NSF under Grant No. DMR-2103958. This research also used resources of the Oak Ridge Leadership Computing Facility, which is supported by the Office of Science of the U.S. Department of Energy under Contract No. DE-AC05-00OR22725. This research was supported in part by an appointment to the Oak Ridge National Laboratory GRO Program, sponsored by the U.S. Department of Energy and administered by the Oak Ridge Institute for Science and Education. The authors would like to thank D. Nicholson for providing helpful comments.

-
- [1] D. B. Miracle and O. N. Senkov, A critical review of high entropy alloys and related concepts, *Acta Mater.* **122**, 448 (2017).
- [2] M. M. Trexler and N. N. Thadhani, Mechanical properties of bulk metallic glasses, *Prog. Mater. Sci.* **55**, 759 (2010).
- [3] A. Goldman and M. Widom, Quasicrystal structure and properties, *Annu. Rev. Phys. Chem.* **42**, 685 (1991).
- [4] D. Lin, L. Xu, X. Li, H. Jing, G. Qin, H. Pang, and F. Minami, A Si-containing FeCoCrNi high-entropy alloy with high strength and ductility synthesized *in situ* via selective laser melting, *Addit. Manuf.* **35**, 101340 (2020).
- [5] Z. Lei, X. Liu, Y. Wu, H. Wang, S. Jiang, S. Wang, X. Hui, Y. Wu, B. Gault, P. Kontis, D. Raabe, L. Gu, Q. Zhang, H. Chen, H. Wang, J. Liu, K. An, Q. Zeng, T. Nieh, and Z. Lu, Enhanced strength and ductility in a high-entropy alloy via ordered oxygen complexes, *Nature (London)* **563**, 546 (2018).
- [6] Y. Chen, Y. Fang, R. Wang, Y. Tang, S. Bai, and Q. Yu, Achieving high strength and ductility in high-entropy alloys via spinodal decomposition-induced compositional heterogeneity, *J. Mater. Sci. Technol.* **141**, 149 (2023).
- [7] M. Telford, The case for bulk metallic glass, *Mater. Today* **7**, 36 (2004).
- [8] K. Gao, X. G. Zhu, L. Chen, W. H. Li, X. Xu, B. T. Pan, W. R. Li, W. H. Zhou, L. Li, W. Huang, and Y. Li, Recent development in the application of bulk metallic glasses, *J. Mater. Sci. Technol.* **131**, 115 (2022).
- [9] H. Bakhtiari, M. R. Rahimipour, M. Farvizi, and M. R. Khanzadeh, An overview of quasicrystals, their types, preparation methods, properties, *J. Environ. Friendly Mater.* **5**, 69 (2021).
- [10] R. Li, L. Xie, W. Y. Wang, P. K. Liaw, and Y. Zhang, High-throughput calculations for high-entropy alloys: A brief review, *Front. Mater.* **7**, 290 (2020).
- [11] R. Feng, C. Zhang, M. C. Gao, Z. Pei, F. Zhang, Y. Chen, D. Ma, K. An, J. D. Poplawsky, L. Ouyang, Y. Ren, J. A. Hawk, M. Widom, and P. K. Liaw, High-throughput design of high-performance lightweight high-entropy alloys, *Nat. Commun.* **12**, 4329 (2021).
- [12] V. Sorkin, Z. G. Yu, S. Chen, T. L. Tan, Z. H. Aitken, and Y. W. Zhang, A first-principles-based high fidelity, high throughput approach for the design of high entropy alloys, *Sci. Rep.* **12**, 11894 (2022).
- [13] P. Soven, Coherent-potential model of substitutional disordered alloys, *Phys. Rev.* **156**, 809 (1967).
- [14] Y. Wang, G. M. Stocks, W. A. Shelton, D. M. C. Nicholson, Z. Szotek, and W. M. Temmerman, Order- N multiple scattering approach to electronic structure calculations, *Phys. Rev. Lett.* **75**, 2867 (1995).
- [15] J. Korringa, On the calculation of the energy of a Bloch wave in a metal, *Physica* **13**, 392 (1947).
- [16] W. Kohn and N. Rostoker, Solution of the Schrödinger equation in periodic lattices with an application to metallic lithium, *Phys. Rev.* **94**, 1111 (1954).
- [17] M. Eisenbach, J. Larkin, J. Lutjens, S. Rennich, and J. H. Rogers, GPU acceleration of the locally selfconsistent multiple scattering code for first principles calculation of the ground state and statistical physics of materials, *Comput. Phys. Commun.* **211**, 2 (2017).
- [18] R. Kubo, Statistical-mechanical theory of irreversible processes. I. General theory and simple applications to magnetic and conduction problems, *J. Phys. Soc. Jpn.* **12**, 570 (1957).
- [19] D. A. Greenwood, The Boltzmann equation in the theory of electrical conduction in metals, *Proc. Phys. Soc.* **71**, 585 (1958).
- [20] W. H. Butler, Theory of electronic transport in random alloys: Korringa-Kohn-Rostoker coherent-potential approximation, *Phys. Rev. B* **31**, 3260 (1985).
- [21] J. C. Swihart, W. H. Butler, G. M. Stocks, D. M. Nicholson, and R. C. Ward, First-principles calculation of the residual electrical resistivity of random alloys, *Phys. Rev. Lett.* **57**, 1181 (1986).
- [22] S. Mu, G. D. Samolyuk, S. Wimmer, M. C. Tropicovsky, S. N. Khan, S. Mankovsky, H. Ebert, and G. M. Stocks, Uncovering electron scattering mechanisms in NiFeCoCrMn derived concentrated solid solution and high entropy alloys, *npj Comput. Mater.* **5**, 1 (2019).
- [23] V. Raghuraman, Y. Wang, and M. Widom, An investigation of high entropy alloy conductivity using first-principles calculations, *Appl. Phys. Lett.* **119**, 121903 (2021).
- [24] <https://github.com/mstsuite/lsm>.
- [25] P. Hohenberg and W. Kohn, Inhomogeneous electron gas, *Phys. Rev.* **136**, B864 (1964).
- [26] W. Kohn and L. J. Sham, Self-consistent equations including exchange and correlation effects, *Phys. Rev.* **140**, A1133 (1965).

- [27] J. S. Faulkner and G. M. Stocks, Calculating properties with the coherent-potential approximation, *Phys. Rev. B* **21**, 3222 (1980).
- [28] J. S. Faulkner, G. M. Stocks, and Y. Wang, *Multiple Scattering Theory* (IOP Publishing, Bristol, UK, 2018).
- [29] B. Györfy and M. Stott, in *Band Structure Spectroscopy of Metals and Alloys*, edited by D. J. Fabian and L. M. Watson (Academic, New York, 1973), p. 385.
- [30] U. von Barth and L. Hedin, A local exchange-correlation potential for the spin polarized case: I, *J. Phys. C: Solid State Phys.* **5**, 1629 (1972).
- [31] <https://github.com/mstsuite/MuST>.
- [32] A. F. Ioffe and A. R. Regel, Non-crystalline, amorphous and liquid electronic semiconductors, *Prog. Semicond.* **4**, 237 (1960).
- [33] N. E. Alekseevskii, A. V. Mitin, and N. M. Matveeva, Investigation of the superconducting properties of V-Al and V-Sn solid solutions, *Zh. Eksp. Teor. Fiz.* **69**, 2124 (1975).
- [34] C. T. Seagle, E. Cottrell, Y. Fei, D. R. Hummer, and V. B. Prakapenka, Electrical and thermal conductivity of iron and iron-silicon alloy at high pressures, *Geophys. Res. Lett.* **40**, 5377 (2013).